THE JOURNAL OF BIOLOGICAL CHEMISTRY Vol. 277, No. 44, Issue of November 1, pp. 42289–42298, 2002
Printed in U.S.A.

Solution Structure of the Phosphoryl Transfer Complex between the Cytoplasmic A Domain of the Mannitol Transporter II^{Mannitol} and HPr of the *Escherichia coli* Phosphotransferase System*

Received for publication, July 20, 2002, and in revised form, August 26, 2002
Published, JBC Papers in Press, August 28, 2002, DOI 10.1074/jbc.M207314200

Gabriel Cornilescu‡§, Byeong Ryong Lee¶, Claudia C. Cornilescu‖, Guangshun Wang‡, Alan Peterkofsky¶, and G. Marius Clore‡

From the ‡Laboratory of Chemical Physics, NIDDK, and Laboratories of ¶Cell Biology and ‖Biophysical Chemistry, NHLBI, National Institutes of Health, Bethesda, Maryland 20892

The solution structure of the complex between the cytoplasmic A domain (IIA^{Mtl}) of the mannitol transporter II^{Mannitol} and the histidine-containing phosphocarrier protein (HPr) of the *Escherichia coli* phosphotransferase system has been solved by NMR, including the use of conjoined rigid body/torsion angle dynamics, and residual dipolar couplings, coupled with cross-validation, to permit accurate orientation of the two proteins. A convex surface on HPr, formed by helices 1 and 2, interacts with a complementary concave depression on the surface of IIA^{Mtl} formed by helix 3, portions of helices 2 and 4, and β-strands 2 and 3. The majority of intermolecular contacts are hydrophobic, with a small number of electrostatic interactions at the periphery of the interface. The active site histidines, *His-15* of HPr and His-65 of IIA^{Mtl}, are in close spatial proximity, and a pentacoordinate phosphoryl transition state can be readily accommodated with no change in protein-protein orientation and only minimal perturbations of the backbone immediately adjacent to the histidines. Comparison with two previously solved structures of complexes of HPr with partner proteins of the phosphotransferase system, the N-terminal domain of enzyme I (EIN) and enzyme IIA^{Glucose} (IIA^{Glc}), reveals a number of common features despite the fact that EIN, IIA^{Glc}, and IIA^{Mtl} bear no structural resemblance to one another. Thus, entirely different underlying structural elements can form binding surfaces for HPr that are similar in terms of both shape and residue composition. These structural comparisons illustrate the roles of surface and residue complementarity, redundancy, incremental build-up of specificity and conformational side chain plasticity in the formation of transient specific protein-protein complexes in signal transduction pathways.

The bacterial phosphoenolpyruvate:sugar phosphotransferase system (1) is a classical example of a signal transduction pathway whereby the transfer of a phosphoryl group through a series of bimolecular protein-protein complexes is coupled with the transport of sugars across the membrane (2–4). The initial events of the cascade involve a common pathway: enzyme I, which is autophosphorylated by phosphoenolpyruvate at His-189 (in *Escherichia coli*), transfers the phosphoryl group to His-15 (in *E. coli*) of the histidine-containing phosphocarrier protein (HPr).[1] Subsequently, the phosphoryl group on HPr is transferred to a variety of sugar-specific carbohydrate transporters, known as enzymes II (5). The enzymes II are organized into several domains, some of which are covalently linked (5). There are two cytoplasmic domains, IIA and IIB; IIA accepts the phosphoryl group from HPr and then transfers it to IIB. The transmembrane domain IIC (and in some cases IID as well) catalyzes the translocation and phosphoryl transfer from IIB to the incoming sugar. There are five classes of enzymes II as follows: glucose-sucrose, mannitol-fructose, mannose-sorbose, lactose-cellobiose, and glucitol (3, 5). The membrane-bound IIC domains comprise a variable number of transmembrane helices (5). The IIA and IIB domains for the different sugar classes bear no sequence or structural similarity to one another (6–15).

The bacterial phosphoenolpyruvate:sugar phosphotransferase system provides a paradigm for understanding protein-protein interactions and the factors governing their specificity. Thus, for example, HPr recognizes enzyme I and the various sugar-specific IIA domains, although all these target proteins are structurally dissimilar. We have recently solved the structures of the complexes between the N-terminal phosphoryl transfer domain of EI (EIN) and HPr (16) and between IIA^{Glucose} (IIA^{Glc}) and HPr (17). In the present paper, we extend these studies to the solution structure determination of the complex between IIA^{Mannitol} (IIA^{Mtl}) and HPr.

EXPERIMENTAL PROCEDURES

Expression Vector for IIA^{Mtl}—E. coli chromosomal DNA was used as a template to amplify by PCR the region corresponding to the A domain of the mannitol permease. The forward PCR primer 5′-GACAGCTTTGACGATCATATGGCTAACCTGTTCAAG-3′ contained an engineered *Nde*I restriction site (underlined), and the reverse primer 5′-TTAACCCCACCTTCTCCATGTCGACAGGGTGGGATTGG-3′ contained an engineered *Sal*I site (underlined). The *Nde*I- and *Sal*I-cut PCR product was purified and cloned into the corresponding sites of the vector pRE1

* This work was supported in part by the Intramural AIDS Targeted Antiviral Program of the Office of the Director of the National Institutes of Health (to G. M. C.). The costs of publication of this article were defrayed in part by the payment of page charges. This article must therefore be hereby marked "*advertisement*" in accordance with 18 U.S.C. Section 1734 solely to indicate this fact.

The atomic coordinates and experimental NMR restraints (code 1J6T) have been deposited in the Protein Data Bank, Research Collaboratory for Structural Bioinformatics, Rutgers University, New Brunswick, NJ (http:/www.rcsb.org/).

§ Recipient of a PRAT postdoctoral fellowship from NIGMS, National Institutes of Health.

** To whom correspondence should be addressed: Laboratory of Chemical Physics, Bldg. 5, Rm. B1-30I, NIDDK, National Institutes of Health, Bethesda, MD 20892-0510. Tel.: 301-496-0782; Fax: 301-496-0825; E-mail: mariusc@intra.niddk.nih.gov.

[1] The abbreviations used are: HPr, histidine-containing phosphocarrier protein; EI, enzyme I; EIN, N-terminal domain of enzyme I; IIA^{Mtl}, cytoplasmic A domain of the mannitol-specific transporter II^{Mannitol}; IIA^{Glc}, glucose-specific enzyme IIA; NOE, nuclear Overhauser effect; r.m.s., root mean square.

(18). The expressed product from the recombinant plasmid (pLP1572) was identical in sequence to that from the clone described by Van Weeghel *et al.* (19).

Protein Expression—The recombinant plasmids, pSP100 for HPr expression (20) and pLP1572 for IIA^{Mtl} expression, were introduced into *E. coli* GI698 for protein expression induced by tryptophan (21). Four-liter cultures were grown in minimal labeling medium (MLM) (22) supplemented with ampicillin (100 μg/ml). For labeling with [$^{13}C_6$]glucose and/or $^{15}NH_4Cl$, the media contained 2.5 gm of [$^{13}C_6$]glucose/liter and/or 1 g of $^{15}NH_4Cl$/liter, respectively. Induction was continued overnight.

Protein Purification—E. coli HPr, unlabeled and/or isotopically labeled with ^{15}N (>95%) and ^{13}C (>95%), was purified as described elsewhere (17, 23).

The 148 residue IIA^{Mtl} domain, containing a methionine residue in front of alanine 491, was purified as follows. Washed cells from a 4-liter culture were suspended in 40 ml of 10 mM Tris-HCl (pH 7.5), 1 mM EDTA (Buffer A). The cell suspension was passed twice through a French press at 10,000 pounds/square inch. The ruptured cells were centrifuged at 100,000 $\times$ *g* for 1 h. The supernatant fraction was applied to a DE52 anion-exchange column (1.5 $\times$ 40 cm) equilibrated with 20 mM Tris-HCl (pH 8.5), 1 mM dithiothreitol (Buffer E). The column was washed with 100 ml of Buffer E supplemented with 100 mM NaCl (Buffer EE). Then a linear gradient (from 500 ml of Buffer EE to 500 ml of Buffer E + 400 mM NaCl (Buffer F)) was run. Column fractions were screened by SDS-PAGE. Fractions enriched in IIA^{Mtl} were pooled and concentrated by ultrafiltration through Filtron 3K membranes. Further purification was achieved by gel filtration chromatography on an AcA-44 Ultrogel column (2.6 $\times$ 100 cm) run with 10 mM Tris-HCl (pH 7.5) + 100 mM NaCl. Fractions enriched in IIA^{Mtl} were pooled and concentrated as before. All protein samples used for the NMR studies were greater than 95% pure, as judged by both SDS-PAGE and two-dimensional ^1H-^{15}N correlation spectra.

The majority of NMR samples contained 1–2 mM 1:1 IIA^{Mtl}-HPr complex in 10 mM phosphate buffer, pH 7.0. The following samples were employed (only the presence of ^{15}N and ^{13}C isotopes are indicated; if no C or N isotope is mentioned, then the sample contained ^{12}C or ^{14}N at natural isotopic abundance): IIA^{Mtl}-HPr(^{15}N), IIA^{Mtl}(^{15}N)-HPr, IIA^{Mtl}-HPr(^{15}N/^{13}C), IIA^{Mtl}(^{15}N/^{13}C)-HPr, IIA^{Mtl}(^{13}C)-HPr(^{15}N), and IIA^{Mtl}(^{15}N)-HPr(^{13}C).

NMR Spectroscopy—All spectra were recorded at 35 °C on Bruker DMX500, DMX600, DMX750, and DRX800 spectrometers equipped with x,y,z-shielded gradient triple resonance probes. Spectra were processed with the NMRPipe package (24) and analyzed using the programs NMRDraw and NMRWish (24), and PIPP, CAPP, and STAPP (25). ^1H, ^{15}N, and ^{13}C sequential assignments were obtained using three-dimensional double and triple resonance through bond correlation experiments (26–28). Three-dimensional experiments employed for sequential assignments included HNCACB, CBCA(CO)NH, HBHA(CBCACO)NH, H(CCO)NH, C(CCO)NH, and HCCH-TOCSY experiments. $^3J_{N\text{-}C\gamma}$, $^3J_{C'\text{-}C\gamma}$, and $^3J_{C\alpha\text{-}C\delta}$ couplings were measured using quantitative *J* correlation spectroscopy (29–31). Interproton distance restraints were derived from multidimensional NOE spectra recorded with mixing times ranging from 75 to 120 ms. NOE experiments included three-dimensional ^{15}N-separated, ^{13}C-separated, and ^{13}C-separated/^{12}C-filtered NOE spectra, and two-dimensional ^{15}N-separated/^{13}C-filtered, ^{15}N-filtered/^{13}C-separated, and ^{13}C-filtered/^{15}N-filtered NOE spectra (26).

Residual $^1D_{NH}$, $^1D_{C\alpha H\alpha}$, and $^1D_{NC'}$ dipolar couplings were obtained by taking the difference in the corresponding *J* splittings measured in magnetically oriented and isotropic (in water) media. The orienting liquid crystalline medium employed consisted of a 4–5% C12E5 polyethylene glycol (PEG)/hexanol mixture with a surfactant to alcohol ratio of 0.96 (32). $^1D_{NH}$ couplings were measured on IIA^{Mtl}-HPr(^{15}N) and IIA^{Mtl}(^{15}N)-HPr complexes using two-dimensional in-phase/anti-phase {^{15}N,^1H} heteronuclear single quantum coherence experiments (33). $^1D_{C\alpha H\alpha}$ and $^1D_{NC'}$ couplings were measured on IIA^{Mtl}-HPr(^{15}N/^{13}C) and IIA^{Mtl}(^{15}N/^{13}C)-HPr complexes using three-dimensional (HCACO)NH and (TROSY)HNCO experiments (34), respectively. In all cases the concentration of labeled protein ranged from 0.6 to 1.0 mM, and the unlabeled protein was present in sufficient excess to ensure that the labeled protein was entirely in the bound state. The $^1D_{NH}$ dipolar couplings were measured in 5% PEG/hexanol using a different stock of PEG/hexanol from the $^1D_{C\alpha H\alpha}$ and $^1D_{NC'}$ dipolar couplings (which were measured in 4% PEG/hexanol). Consequently, two alignment tensors were employed: one for the $^1D_{NH}$ couplings and a second for the $^1D_{C\alpha H\alpha}$ and $^1D_{NC'}$ couplings. The magnitude of the alignment tensor (*i.e.* the values of axial component of the tensor, D_a^{NH}, and the rhombicity η) was obtained by singular value decomposition (35, 36) using the x-ray coordinates of free IIA^{Mtl} (1A3A (11)) and HPr (1POH (37)). The values of D_a^{NH} and η, determined in this manner, are −13.3 and 0.43 Hz, respectively, for the $^1D_{NH}$ set of dipolar couplings, and −9.4 and 0.58 Hz, respectively, for the $^1D_{C\alpha H\alpha}$ and $^1D_{NC'}$ couplings. Note that small, unavoidable, variations in the concentration of PEG/hexanol among different samples only result in correspondingly small variations in the value of the axial component of the alignment tensor, D_a^{NH}. The dipolar couplings are appropriately normalized to reflect this.

Structure Calculations—Intermolecular NOE-derived interproton distance restraints were classified into two ranges, 1.8–5.0 and 1.8–6.0 Å (17). Intramolecular NOE-derived interproton distance restraints relating to the interfacial side chains were classified into four ranges as follows: 1.8–2.7, 1.8–3.5, 1.8–5.0, and 1.8–6.0 Å (38). An additional 0.5 Å was added to the upper bound for NOEs involving methyl groups, and distances involving methyl groups and non-stereospecifically assigned protons were represented by a $(\Sigma r^{-6})^{-1/6}$ sum. χ_1 and χ_2 side chain torsion angle restraints were derived from analysis of heteronuclear ^3J couplings and NOE/(rotating frame Overhauser enhancement) experiments (26). Backbone ϕ/ψ restraints for the four variable regions of IIA^{Mtl} were derived from backbone chemical shift data using the program TALOS (39) in conjunction with knowledge of the ranges for these ϕ/ψ angles observed in the four molecules of the crystal structure of free IIA^{Mtl}.

Structures were calculated by conjoined rigid body/torsion angle dynamics (40, 41) using the program Xplor-NIH (42). The target function minimized comprises the experimental NMR restraints (NOE-derived interproton distances, torsion angles, and residual dipolar couplings (43)), a repulsive van der Waals potential for the non-bonded contacts (36), a torsion angle data base potential of mean force (44), and a radius of gyration restraint to ensure optimal interfacial packing (45).

Structures were visualized and analyzed with the programs VMD-XPLOR (46), RIBBONS (47), and GRASP (48). Reweighted atomic density maps were calculated from the ensemble of simulated annealing structures as described previously (49). Amino acid sequence searches and alignments were carried out using the program BLAST (50).

The coordinates and experimental restraints have been deposited in the RCSB Protein Data Bank (PDB accession code 1J6T).

RESULTS AND DISCUSSION

Structure Determination—The physiological form of enzyme II^{Mtl} consists of the three domains, A–C, joined together in a single polypeptide chain by flexible linkers of variable length (51, 52). The membrane-bound IIC^{Mtl} domain is at the N terminus (residues 1–347), followed by the cytoplasmic IIB^{Mtl} (residues 348–489) with the IIA^{Mtl} (residues 490–637) domain at the C terminus (19, 53–56). The isolated IIA^{Mtl} domain is catalytically active and can accept a phosphoryl group from HPr and transfer it to both the isolated IIB^{Mtl} domain as well as IICB^{Mtl} (19, 55). We have solved the structure of the IIA^{Mtl}-HPr complex by multidimensional NMR. For consistency with previous structural work (11, 57, 58), residues 490–637 of II^{Mtl} are numbered 1–148 in the cloned, expressed IIA^{Mtl} domain; hence, in this numbering scheme, the active site histidine (residue 554 in the full-length II^{Mtl} sequence (59, 60)) is located at position 65.

IIA^{Mtl} and HPr are in fast exchange on the chemical shift scale. The equilibrium association constant derived from NMR titration studies by monitoring ^1H-^{15}N cross-peaks of ^{15}N-labeled IIA^{Mtl} upon addition of unlabeled HPr is $\sim 2 \times 10^4$ M^{-1}. The lower limit for the dissociation rate constant, derived from the maximal observed ^1H_N shift between free and bound states, is $\sim$4500 s^{-1}.

A combination of isotopically (^{15}N and/or ^{13}C) labeled proteins was used to simplify the spectra for assignment purposes and to specifically observe intermolecular nuclear Overhauser effects (NOEs) (26). An example of the quality of the data is illustrated in Fig. 1 which shows a series of strips from three-dimensional ^{13}C-separated/^{12}C-filtered NOE spectra in which NOEs are observed specifically from protons attached to ^{13}C on one protein to protons attached to ^{12}C on the other.

High resolution crystal structures of both HPr ((37) code 1POH) and IIA^{Mtl} ((11) code 1A3A) are available and therefore permit the structure of the complex to be solved by conjoined

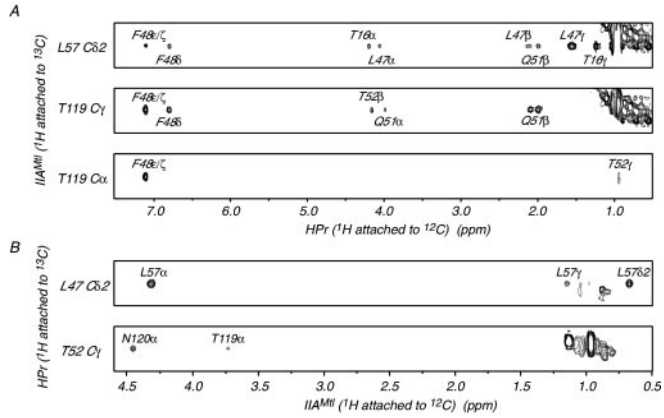

FIG. 1. **Intermolecular NOEs in the IIA^{Mtl}-HPr complex.** Strips from three-dimensional ^{13}C-separated/^{12}C-filtered NOE spectra recorded on a 1:1 IIA^{Mtl}(^{13}C/^{15}N)-HPr(^{12}C/^{14}N) complex (*A*) and IIA^{Mtl}(^{12}C/^{14}N)-HPr(^{13}C/^{15}N) complex (*B*), illustrating specifically intermolecular NOE contacts from protons attached to ^{13}C on one protein to protons attached to ^{12}C on the other. Residues from HPr are denoted in *italics*.

rigid body/torsion angle dynamics (40, 41), in a manner analogous to that employed for the HPr-IIA^{Glc} complex (17). In this approach, it is necessary to either demonstrate that no significant conformational changes occur upon complex formation or to localize regions where such changes may occur. This can be rapidly assessed by the measurement of residual dipolar couplings, which provide highly sensitive long range orientational information (61–65).

For HPr, agreement between observed $^1D_{NH}$ dipolar couplings measured on the complex dissolved in a dilute liquid crystalline medium of polyethylene glycol/hexanol (33) and those calculated from the x-ray structure of free HPr is excellent with a $^1D_{NH}$ dipolar coupling R-factor, R_{dip}^{NH}, of 19.1% and a correlation coefficient of 0.96, consistent with the expected accuracy of a 2-Å resolution crystal structure.

The situation for IIA^{Mtl} is more complex, because the crystal structure has four molecules (A–D) in the unit cell (11): molecules A and B, and molecules C and D are very similar with an overall backbone root mean square difference of ~0.3 Å, consistent with the expected coordinate errors for a 1.8-Å resolution structure. However, the backbone of one region (I, residues 51–54) is displaced by up to ~2 Å in molecule A relative to the other three molecules, and three regions (II, 66–78; III, 91–96; and IV, 104–110) exhibit maximal backbone displacements of up to 1.5–3 Å between the two pairs (A/B and C/D) of structures. Excluding these regions, the backbone root mean square difference between the four structures remains at ~0.3 Å. For the invariant core residues (*i.e.* all residues with the exception of those in the four variable regions), the average values of R_{dip}^{NH} and the correlation coefficients are 20.5 ± 1.2% and 0.96 ± 0.05, respectively, for the four molecules. For the four variable regions, on the other hand, R_{dip}^{NH} and the correlation coefficient have values of 32% and 0.92 for molecule A, 29% and 0.93 for molecule B, 28% and 0.94 for molecule C, and 22% and 0.96 for molecule D. Thus, the overall agreement between the measured and calculated $^1D_{NH}$ dipolar couplings for the four variable regions in molecule D is essentially the same as that of the core residues, whereas the discrepancies for molecules A–C are significantly (~50%) higher. The improvement for molecule D relative to the other three molecules is statistically significant, because it is larger than the intrinsic error, and implies that the structure of molecule D of IIA^{Mtl} is closest to that in the IIA^{Mtl}-HPr complex observed in solution.

Because the variable regions I–IV of IIA^{Mtl} compose several residues (specifically residues 52–54, 68, 92, 93, 96, and 109) at the periphery of the interface with HPr, the following strategy was employed. The starting coordinates comprised the free x-ray structures of *E. coli* HPr (37) and IIA^{Mtl} (molecule D (11)), placed 30–50 Å apart in random orientations. Structures of the complex were calculated from the experimental restraints by rigid body minimization (66), followed by conjoined rigid body/torsion angle dynamics (40, 41). The backbone coordinates and non-interfacial side chains (excluding the four variable regions of IIA^{Mtl}) were treated as rigid bodies throughout, with IIA^{Mtl} held fixed, HPr allowed to rotate and translate, and the axis of the dipolar coupling alignment tensor free to rotate. The interfacial side chains of both IIA^{Mtl} and HPr were given their full torsional degrees of freedom. The backbone and side chains of the four variable regions of IIA^{Mtl} were also given torsional degrees of freedom; the ϕ/ψ angles were restrained by square-well potentials to the ranges covered by all four molecules in the crystal structure of free IIA^{Mtl}, consistent with chemical shift data (39), and the side chain torsion angles of the non-interfacial residues were similarly restrained to the rotamers observed in the crystal structure, consistent with heteronuclear ^3J coupling measurements. In the case of region II, however, residues 64–67 and residues 77–78 were given full torsional degrees of freedom, whereas residues 68–76 were treated as a rigid body because the ϕ/ψ angles for this region differed by less than 5° between all four molecules of the crystal structure. (Note residues 64 and 65 are included in region II to allow appropriate hinge movements to occur.) Within the confines of these torsion angle restraints, the conformations of the four variable regions of IIA^{Mtl} in the complex are determined by the dipolar coupling restraints and intramolecular NOE-derived interproton distance restraints relating to these regions.

The IIA^{Mtl}-HPr complex was solved on the basis of 872 experimental restraints, including 107 intermolecular NOE-derived interproton distance restraints and 528 residual dipolar couplings. A summary of the structural statistics is provided in Tables I and II. A best fit superposition of the backbone for the final ensemble of 200 simulated annealing structures is shown in Fig. 2*A*, and an atomic density map, calculated from the complete ensemble, is shown in Fig. 2*B* to illustrate the distribution of interfacial side chain conformations.

The backbone atomic r.m.s. displacements for variable regions I–IV of IIA^{Mtl} in the complex relative to molecule D of the IIA^{Mtl} crystal structure are small: 0.15, 0.52, 1.09, and 0.48 Å, respectively. The corresponding values relative to molecules A/B/C are 1.50/0.47/0.27, 1.07/1.09/0.59, 0.96/0.66/0.97, and 1.66/1.99/0.66 Å, respectively. Thus, regions I, II, and IV in the complex are closest to molecule D, whereas region III is closest to molecule B.

The dipolar coupling R-factors for the complex, obtained with single alignment tensors for both proteins in the complex, are comparable with those of the free x-ray structures calculated using individual alignment tensors for each protein (Table I). Thus, one can conclude that the relative orientation of the two proteins is uniquely defined by the rotational and translational information afforded by the intermolecular NOE-derived interproton distance restraints and the orientational information afforded by the dipolar couplings (66).

To assess further the accuracy of the relative orientation of the two proteins in the complex, we carried out cross-validation using the dipolar couplings (67). This also probes the effects of errors in the coordinates. The $^1D_{NH}$, $^1D_{C\alpha H}$, and $^1D_{NC'}$ dipolar couplings for each protein were randomly divided into two groups of equal size (A and B). In the first set of calculations, group A was used as the work set and B as the test set; the groups were reversed in the second set of calculations. Only the dipolar couplings in the work set are refined against. Compar-

TABLE I
Structural statistics

The notation of the NMR structures are as follows: ⟨SA⟩ are the final 200 simulated annealing structures; ($\overline{SA}$)r is the restrained regularized mean structure. The number of terms for the various restraints is given in parentheses.

	⟨SA⟩		($\overline{SA}$)r
Number of experimental restraints			
Intermolecular interproton distance restraints		107	
Intramolecular interproton distance restraints[a]		105	
Interfacial side chain torsion angle restraints[a]		70	
Torsion angle restraints for the variable regions of IIA^{Mtl}[a]		62	
Residual dipolar couplings		528	
R.m.s deviation from interproton distance restraints (Å)[b]	0.006 ± 0.001		0.007
R.m.s deviation from sidechain torsion angle restraints (°)[b]	0.25 ± 0.16		0.26
R.m.s deviation for backbone torsion angle restraints (°)[b]	1.2 ± 1.18		1.2
Overall dipolar coupling R-factors (%)[c]			
$^1D_{NH}$ HPr (71)	19.4 ± 0.02		19.1
$^1D_{NH}$ IIA^{Mtl} (114)	20.0 ± 0.02		19.2
$^1D_{C\alpha H}$ HPr (63)	26.0 ± 0.05		25.9
$^1D_{C\alpha H}$ IIA^{Mtl} (121)	20.8 ± 0.08		18.7
$^1D_{NC'}$ HPr (56)	34.3 ± 0.03		34.0
$^1D_{NC'}$ IIA^{Mtl} (103)	32.8 ± 0.06		32.1
Measures of structure quality[d]			
Intermolecular repulsion energy (kcal · mol^{-1})	8.8 ± 1.5		10.6
Intermolecular Lennard-Jones Energy (kcal · mol^{-1})	−28.8 ± 1.5		−28.2
Coordinate precision (Å)[e]			
Backbone (N, Cα, C, O)	0.09		
Interfacial side chains	0.56		
Backbone of variable regions of IIA^{Mtl}	0.11		
Precision of protein-protein orientation (°)[f]	1.4		

[a] The intramolecular interproton distance restraints relate to the interfacial side chains of IIA^{Mtl} and HPr and to the four variable regions of IIA^{Mtl}; there are 24 intraresidue restraints and 40 sequential ($|i-j| = 1$), 21 medium range ($1 < |i-j| < 5$), and 20 long range ($|i-j| > 5$) interresidue restraints. In addition to the side chain torsion angle restraints related to the interfacial side chains, 23 ϕ, 23 ψ, and 16 side chain torsion angle restraints related to the variable regions of IIA^{Mtl} were also included in the calculations (see text).

[b] None of the structures exhibited interproton distance violations >0.2 Å or torsion angle violations >5°.

[c] The dipolar coupling R-factor is defined as the ratio of the r.m.s. deviation between observed and calculated values to the expected r.m.s. deviation if the vectors were randomly oriented. The latter is given by $\{2D_a^2[4 + 3\eta^2]/5\}^{1/2}$, where D_a is the magnitude of the axial component of the alignment tensor and η the rhombicity (67). D_a^{NH} and η have values of −13.3 Hz and 0.43, respectively, for the $^1D_{NH}$ set of dipolar couplings, and −9.4 Hz and 0.58, respectively, for the $^1D_{C\alpha H}$ and $^1D_{NC'}$ set of dipolar couplings. For reference, the $^1D_{NH}$, $^1D_{C\alpha H}$, and $^1D_{NC'}$ dipolar coupling R-factors are 19.1, 25.2, and 34.1%, respectively, for the free x-ray structure of HPr (1POH (37)); 21.3, 21.1, and 33.6%, respectively, for the free x-ray structure IIA^{Mtl} (molecule D of 1A3A (11)); and 19.2, 18.0, and 32.0% for the restrained regularized mean structure of IIA^{Mtl} in the complex fitted with an individual alignment tensor for IIA^{Mtl} alone.

[d] The intermolecular repulsion energy is given by the value of the intermolecular quartic van der Waals repulsion term (38) calculated with a force constant of 4 kcal · mol^{-1} · Å^{-2} and a van der Waals radius scale factor of 0.8. The intermolecular Lennard-Jones van der Waals energy is calculated using the CHARMM19/20 parameters and is *not* included in the target function employed in the structure calculations. The percentages of residues present in the most favorable region of the Ramachandran plot (78) are 93 and 92% for the x-ray structures of HPr (1POH) and IIA^{Mtl} (molecule D of 1A3A), respectively, and 92% for the restrained regularized mean structure of IIA^{Mtl} in the complex.

[e] Defined as the average r.m.s. difference between the final 200 simulated annealing structures (calculated with dipolar coupling cross-validation; *cf.* Table II) and the mean coordinates. The value quoted for the complete backbone atoms provides only a measure of the precision with which the relative orientation of the two proteins have been determined and does *not* take into account the accuracy of the x-ray coordinates of HPr (37) and IIA^{Mtl} (11). The latter is expected to be ~0.3 Å, as judged from the crystallographic resolution and R-factors. The four variable regions of IIA^{Mtl} comprise residues 51–54, 64–78, 91–96, and 104–110. (Note residues 64 and 65 are included in region II to allow appropriate hinge movements to occur since residues 68–76 are treated as a rigid body.)

[f] Defined as the average angular r.m.s. difference in the relative orientation of HPr and IIA^{Mtl} between the mean coordinates derived from the simulated annealing structures calculated with all dipolar couplings and those derived from structures obtained in the first and second set of calculations with dipolar coupling cross-validation (Table II).

TABLE II
Dipolar coupling cross-validation

The dipolar couplings, excluding those of the four variable regions of IIA^{Mtl}, were randomly divided into two equal groups, A and B, each comprising 50% of the dipolar couplings. In the Set 1 calculations, group A was used as the work set and group B as the free set; in the Set 2 calculations, group B was used as the work set and group A as the free set. Thus, R_{dip}(work) from Set 1 and R_{dip}(free) from Set 2 comprise the same dipolar couplings; likewise for R_{dip}(free) from Set 1 and R_{dip}(work) from Set 2.

Dipolar couplings[a]	Dipolar coupling R-factor (%)			
	Set 1		Set 2	
	R_{dip}(work)	R_{dip}(free)	R_{dip}(work)	R_{dip}(free)
$^1D_{NH}$ HPr (71)	17.6 ± 0.02	21.8 ± 0.09	20.6 ± 0.04	17.7 ± 0.02
$^1D_{NH}$ IIA^{Mtl} (92)	20.9 ± 0.02	21.7 ± 0.03	21.6 ± 0.01	21.2 ± 0.03
$^1D_{C\alpha H}$ HPr (63)	27.3 ± 0.10	27.3 ± 0.08	27.1 ± 0.07	28.1 ± 0.09
$^1D_{C\alpha H}$ IIA^{Mtl} (101)	18.4 ± 0.08	22.4 ± 0.13	22.0 ± 0.09	19.1 ± 0.11
$^1D_{NC'}$ HPr (56)	35.1 ± 0.02	33.4 ± 0.09	33.5 ± 0.08	35.3 ± 0.03
$^1D_{NC'}$ IIA^{Mtl} (81)	35.8 ± 0.02	30.1 ± 0.07	29.9 ± 0.05	35.9 ± 0.03

[a] The numbers in parentheses refer to the total number of each particular type of dipolar coupling used in cross-validation. In the case of IIA^{Mtl}, the dipolar couplings from the four variable regions (22 $^1D_{NH}$, 20 $^1D_{C\alpha H}$, and 22 $^1D_{NC'}$) are excluded from cross-validation.

ison of the values of the working dipolar coupling R-factors, R_{dip}(work), with the corresponding cross-validated ones, R_{dip}(free), indicates that the values of R_{dip}(work) and R_{dip}(free) from the first and second set of calculations, respectively, are essentially identical, and similarly for R_{dip}(free) and R_{dip}(work) from the first and second set of calculations, respectively (Table

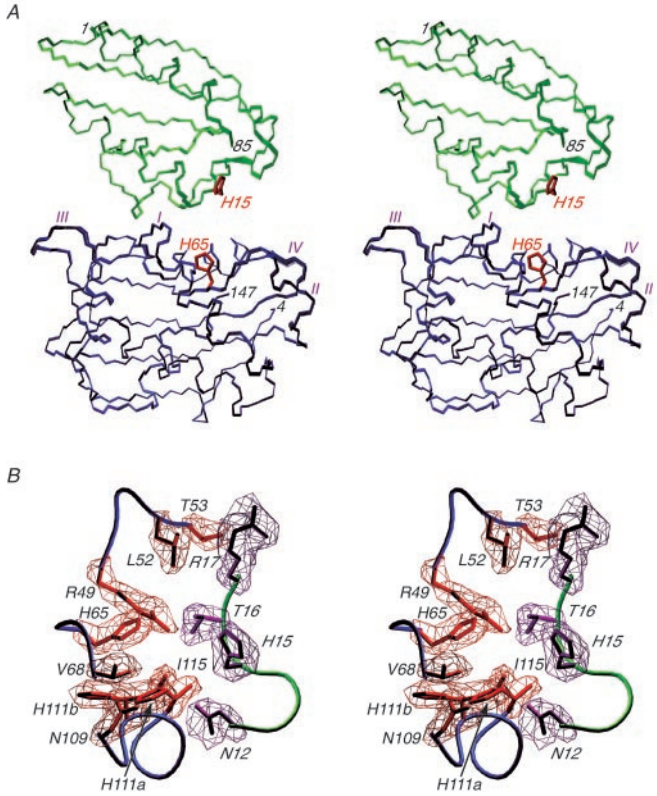

FIG. 2. **The structure of the *E. coli* IIA^{Mtl}-HPr complex.** *A*, best fit superposition of the backbone of the final 200 simulated annealing structures with IIA^{Mtl} in *blue* and HPr in *green*; the side chains of the active site histidines (His-65 of IIA^{Mtl} and *His-15* of HPr) in the restrained regularized mean coordinates are shown in *red*. The location of the four variable regions (*I–IV*) of IIA^{Mtl} are indicated (residues 51–54, 66–78, 91–96, and 104–110). *B*, isosurface of the reweighted atomic density map drawn at a value of 25% of maximum, calculated from the final 200 simulated annealing structures, for selected interfacial side chains of IIA^{Mtl} (*red*) and HPr (*purple*); the backbones of IIA^{Mtl} (*blue*) and HPr (*green*) are displayed as *tubes*. The side chain coordinates displayed within the atomic density map are those of the restrained regularized mean structure; note that the side chain of His-111 of IIA^{Mtl} of HPr is clustered into two populations and was refined as such in the calculation of the restrained regularized mean structure. Residues from HPr are denoted in *italics*.

II). Thus, the quality of the fit to the experimental dipolar coupling data is good, and the dipolar coupling data have not been overfitted (67). Comparison of the relative orientations of the two proteins in these two sets of calculations with that obtained using all the dipolar couplings indicates that the relative orientation of the two proteins is determined with a precision of $\leq$1.5°, which corresponds approximately to the expected uncertainty in the orientation of the dipolar coupling alignment tensor (68). In this regard it is worth noting that there is only a 1.9° difference in orientation between the alignment tensor used for the $^1D_{NH}$ couplings obtained from one stock of PEG/hexanol and that used for the $^1D_{C\alpha H\alpha}$ and $^1D_{NC'}$ couplings obtained from a different PEG/hexanol stock. The backbone r.m.s. difference between the mean coordinates derived from the first and second set of cross-validation calculations and those obtained with all dipolar couplings is $\leq$0.1 Å, which is comparable with the precision of the backbone coordinates.

As indicated above, one alignment tensor was employed for the $^1D_{NH}$ dipolar couplings and another for the $^1D_{C\alpha H\alpha}$ and $^1D_{NC'}$ couplings because different stocks of PEG/hexanol were used to measure these two sets of dipolar couplings. If the calculations are repeated using a single alignment tensor with an average value for the rhombicity and all the dipolar couplings normalized to a single D_a^{NH} value, the difference in relative protein-protein orientation is only 1.7° with a backbone atomic r.m.s. difference of 0.15 Å. This provides an upper limit estimate of the uncertainty in the relative protein-protein orientation introduced by inaccuracies in the value of the rhombicity.

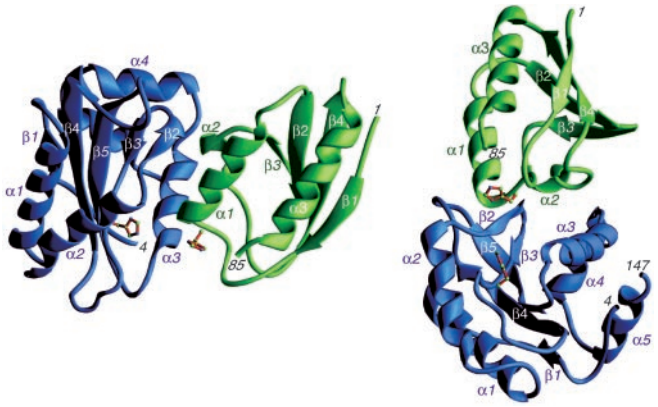

FIG. 3. **Ribbon diagram showing two views of the *E. coli* IIA^{Mtl}-HPr complex.** IIA^{Mtl} is in *blue* and HPr in *green*; the side chains of the active site histidines (His-65 of IIA^{Mtl} and *His-15* of HPr) are also shown (*red*). Residues from HPr are labeled in *italics*. The secondary structure elements are indicated.

It should also be noted that the difference in relative protein-protein orientation for the structures calculated as described above with those calculated using molecules A or D of the crystal structure of IIA^{Mtl} with their backbones held rigid differ by only 1.8 and 0.9°, respectively. This provides a measure of the uncertainty in the determination of the relative protein-protein orientation introduced by inaccuracies in the crystal structure coordinates.

A final check on quality is afforded by calculations omitting all dipolar coupling restraints. The resulting values of R_{dip} are on average only ~3% higher than those obtained when all the dipolar couplings are included in the structure calculation, the difference in relative orientation for the two proteins between the mean coordinates calculated with and without dipolar couplings is ~5°, and the corresponding backbone r.m.s. difference is ~0.5 Å.

Overall Description of the IIA^{Mtl}-HPr Interface—Two views of the overall IIA^{Mtl}-HPr complex, displayed as ribbon diagrams, are shown in Fig. 3 (throughout the text and figures, residues of HPr are denoted in *italics*). The IIA^{Mtl} binding surface on HPr is convex and comprises two segments of the polypeptide chain (residues 12–27 and 46–56) encompassing helices α1 (residues 16–28) and α2 (residues 47–52), consistent with previous chemical shift mapping studies (69). HPr docks into a concave cleft on the surface of IIA^{Mtl} formed by three distinct segments of polypeptide chain as follows: residues 49–68 that include the C-terminal end of helix α2 (residues 41–52), an antiparallel β-sheet formed by β-strands 2 (residues 56–58) and 3 (residues 61–62), and the active site histidine at position 65; residues 92, 93, and 96 located in the loop connecting β-strands 4 and 5; and residues 109–128 that includes helix α3 (residue 111–121) and the N-terminal portion of helix α4 (residues 125–133). The interface is ~27 Å long and ~22 Å wide and comprises a total of 42 residues, 25 from IIA^{Mtl} and 17 from HPr. The interfacial residues are distributed between ~60% non-polar residues and ~40% polar ones. The total accessible surface area buried upon complexation is ~1450 Å^2 of which 685 Å^2 originate from IIA^{Mtl} and ~765 Å^2 from HPr.

A detailed view of the interface is shown in Fig. 4*A* together with a diagrammatic summary of the intermolecular contacts

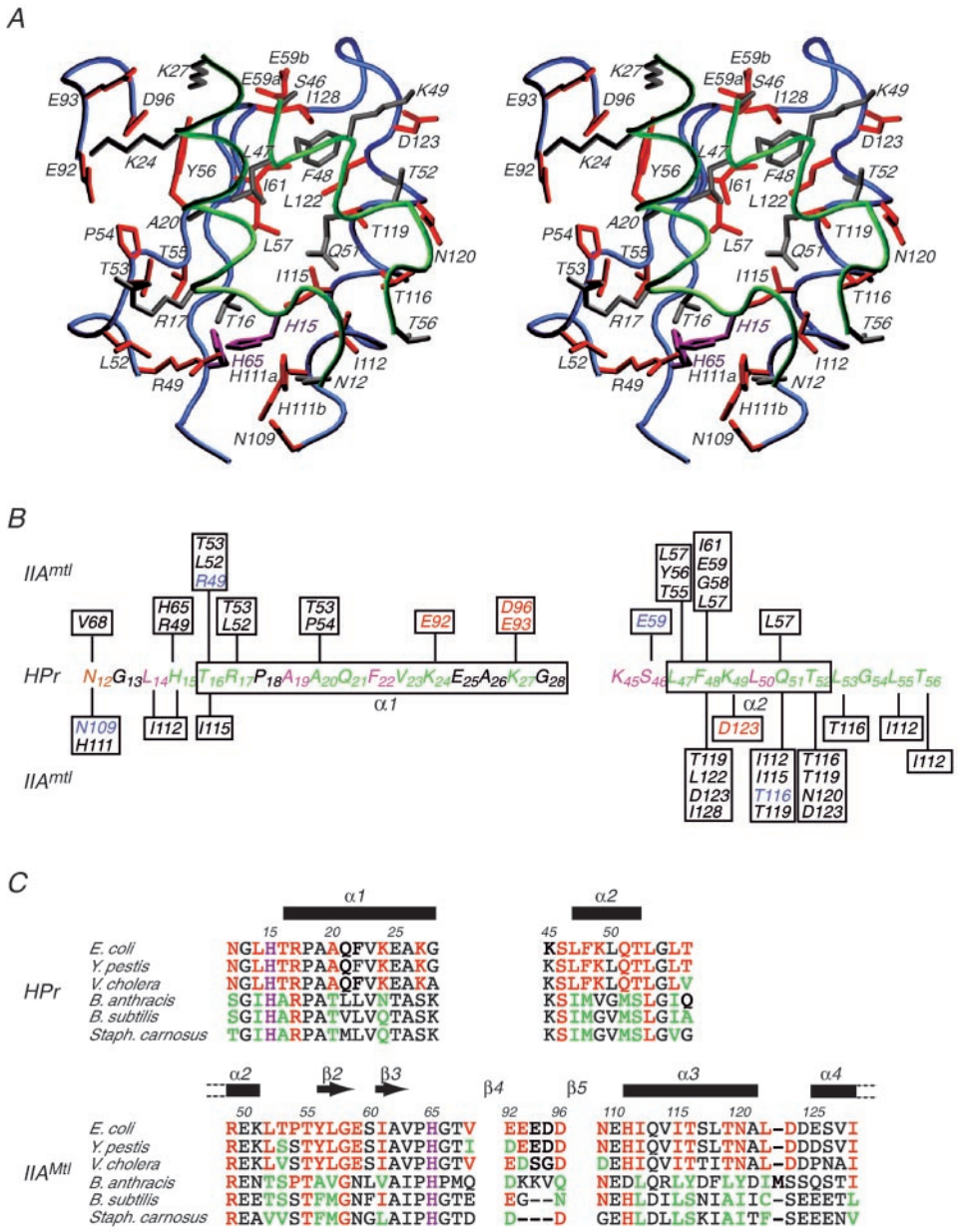

FIG. 4. **Interactions at the interface of the IIA^{Mtl}-HPr complex.** *A*, stereoview of the IIA^{Mtl}-HPr interface. The backbones of IIA^{Mtl} and HPr, depicted as *tubes*, are shown in *blue* and *green*, respectively; the side chains of IIA^{Mtl} and HPr are shown in *red* and *gray*, respectively, and the active site histidines (His-65 of IIA^{Mtl} and *His-15* of HPr) are depicted in *purple.* Residues from HPr are labeled in *italics. B*, diagrammatic summary of interfacial contacts. Side chains of IIA^{Mtl} depicted in *red* and *blue* are involved in potential (direct or water-mediated) electrostatic and hydrogen-bonding interactions, respectively, with the indicated residue on HPr. Residues of HPr depicted in *green* also participate in the interfaces of both the *E. coli* EIN-HPr (16) and IIA^{Glc}-HPr (17) complexes; HPr residues in *purple* are located at the interface of the EIN-HPr complex but not the IIA^{Glc}-HPr complex, and vice versa for HPr residues in *orange. C*, sequence comparison of interfacial residues of HPr and IIA^{Mtl} for Gram-negative (*E. coli*, *Y. pestis*, and *V. cholera*) and positive (*B. anthracis*, *B. subtilis*, and *S. carnosus*) bacteria. The active site histidines are shown in *purple*; the other interfacial residues in *E. coli* are shown in *red* and *boldface*; for the proteins of the other bacteria, interfacial residues that are identical are shown in *red* and those that are conservatively substituted (defined in terms of preserving a similar intermolecular interaction) are shown in *green.* The overall percentage sequence identities relative to the complete *E. coli* HPr and IIA^{Mtl} sequences are 97/86% for *Y. pestis*, 76/65% for *V. cholera*, 40/28% for *B. anthracis*, 35/42% for *B. subtilis*, and 34/41% for *S. carnosus*; the percentage sequence identities relative to the interfacial residues of HPr (17 residues) and IIA^{Mtl} (25 residues) are 100/83% for *Y. pestis*, 94/79% for *V. cholera*, 24/29% for *B. anthracis*, 24/38% for *B. subtilis*, and 24/21% for *S. carnosus*.

in Fig. 4*B*. The majority of interactions are hydrophobic in nature. The most extensive of these involves the aromatic ring of *Phe48* of HPr which is surrounded by a hydrophobic cluster of residues on IIA^{Mtl} including Leu-57, Gly-58, Ile-61, Thr-119, Leu-122, and Ile-128. In addition, there are several potential electrostatic and/or hydrogen bonding interactions (either direct or water-mediated) between the side chains of *Asn-12* and Asn-109, *Thr-16* and Arg-49, *Lys-24* and Glu-92, *Lys-27* and Glu-93/Asp-96, *Ser-46* and Glu-59, *Lys-49* and Asp-123, and *Gln-51* and Thr-116.

The conformations of two side chains, His-111 and Glu-59 of IIA^{Mtl}, cluster into two distinct conformations. For His-111, the g^+ and g^- χ_1 rotamers (labeled *a* and *b*, respectively, in both Figs. 2*B* and 4*A*) are approximately equally populated. This is consistent both with previous NMR measurements on free IIA^{Mtl} which indicated the presence of two conformations for His-111 in slow exchange (57), as well as with the observation of two alternate conformations in different molecules of the crystal structure of free IIA^{Mtl} (11). In the case of Glu-59, the χ_2 angle is ~70% in the g^- rotamer (conformer *a*) and ~30% in the

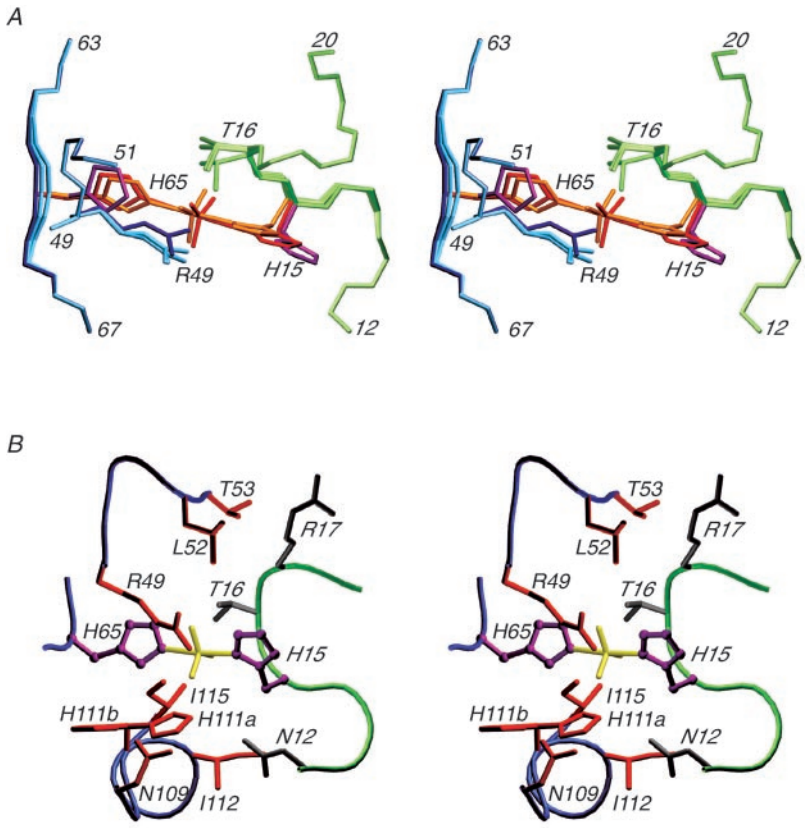

FIG. 5. **The transition state of the IIA^{Mtl}-P-HPr complex.** *A*, detailed view around the active site histidines, illustrating the backbone and side chain positions in the unphosphorylated complex, the dissociative transition state, and the associative transition state. The backbones of IIA^{Mtl} and HPr are shown in *dark blue* and *dark green*, respectively, for the unphosphorylated complex, and in *light blue* and *light green*, respectively, for the putative dissociative and associative transition states; the active site histidines and pentacoordinate phosphoryl group (in the case of the transition states) are shown in *purple* for the unphosphorylated complex, in *red* for the dissociative transition state (Nϵ2-*Nδ1* distance of ~6 Å between His-65 and *His-15*), and in *orange* for the associative transition state (Nϵ2–*Nδ1* distance of ~4 Å between His-65 and *His-15*). Small changes in the backbone of residues 64–66 of IIA^{Mtl} and residues *14–16* of HPr are required to accommodate the transition states. *B*, detailed view of the active site in the putative transition state illustrating the interactions that stabilize the phosphoryl group. The color coding is as follows: the backbone and side chains of IIA^{Mtl} are shown in *blue* and *red*, respectively; the backbone and side chains of HPr are shown in *green* and *gray*, respectively; the active site histidines are in *purple*, and the pentacoordinate phosphoryl group is in *yellow*. Residues from HPr are labeled in *italics*.

g^+ rotamer (conformer *b*). In the minor *b* conformer, the carboxylate of Glu-59 is within hydrogen bonding distance of the hydroxyl group of *Ser-46* (Fig. 4*A*). In the major *a* conformer, Glu-59 can still potentially interact indirectly with *Ser-46* via a water-bridged molecule (Fig. 4*A*).

Some degree of assessment of the relative importance of the various intermolecular interactions can be gauged by sequence comparisons of the interfacial residues of IIA^{Mtl} and HPr among a variety of bacterial species. The species chosen comprise examples of Gram-negative (*Yersinia pestis* and *Vibrio cholera*) and Gram-positive (*Bacillus anthracis*, *Bacillus subtilis*, and *Staphylococcus carnosus*) bacteria, and the sequence alignments are shown in Fig. 4*C*. The overall sequence identities for the complete protein sequences range from 28 to 97% relative to the *E. coli* sequences (50). In the case of the Gram-negative bacteria, *E. coli*, *Y. pestis*, and *V. cholera*, sequence conservation among the interfacial residues is higher than that for the overall proteins. In addition, the few substitutions are highly conservative in terms of the intermolecular interactions in which they participate. Thus, for example, substitution of *Thr-56* of HPr by *Val* in *V. cholera* still permits hydrophobic interactions with Ile-112 of IIA^{Mtl}; likewise, substitution of Thr-53 in IIA^{Mtl} by Ser in *Y. pestis* and Val in *V. cholera* maintains hydrophobic interactions with the aliphatic portion of the side chain of *Arg-17* and the methyl group of *Ala-20* of HPr. However, it seems likely that the potential salt bridges involving *Lys-24* and *Lys-27* of HPr and Glu-92, Glu-93, and Asp-96 of IIA^{Mtl} seen in the *E. coli* complex may not be that critical, because Glu-92 and Glu-93 are substituted by a shorter Asp side chain in *Y. pestis* and *V. cholera* IIA^{Mtl}, respectively. Nevertheless, these substitutions at positions 92 and 93 in *Y. pestis* and *V. cholera*, respectively, would still permit water-bridged electrostatic interactions at the periphery of the interface.

Sequence conservation between the *E. coli* proteins and those of the Gram-positive bacteria, *B. anthracis*, *B. subtilis*, and *S. carnosus*, is lower, ranging from 28 to 42% overall and 21 to 38% for the interfacial residues (Fig. 4*C*). These sequence comparisons highlight the critical importance of the intermolecular hydrophobic interactions involving the side chains of residues *16* (*Thr or Ala*), *17* (*Arg*), *47* (*Leu or Ile*), *48* (*Phe or Met*), and *51* (*Gln or Met*) of HPr and the side chains of residues 52 (Leu, Thr, or Val), 57 (Leu, Met, or Val), 112 (Ile or Leu), 115 (Ile or Leu), 119 (Thr, Ala, or Leu) and 122 (Leu, Phe, Ile, or Cys) of IIA^{Mtl}. The intermolecular electrostatic interactions observed in the *E. coli* complex, however, are much less conserved, suggesting that these are not critical determinants of specificity. Thus, the salt bridge between *Lys-49* of HPr and Asp-123 of IIA^{Mtl} in the *E. coli* complex is abrogated by substitution of *Lys-49* to an aliphatic side chain (*Val* or *Gly*) and Asp-123 to a neutral Ser. Salt bridges involving *Lys-24*/*Lys-27* and Glu-92/Glu-93/Asp-96 in the *E. coli* complex can no longer occur because of substitution of the two lysines to neutral residues (*Gln* or *Asn* at position *24* and *Ser* at position *27*), although water-bridged hydrogen bonding interactions are still possible. The probable water-mediated hydrogen bonding interaction between residue *12* (*Asn*, *Thr* or *Ser*) of HPr and 109 (Asn or Asp) of IIA^{Mtl} does appear to be preserved except in the case of *S. carnosus* where Asn-109 is replaced by a Gly.

Although many features of the HPr and IIA^{Mtl} interfaces are preserved between the Gram-negative and -positive bacteria, there is still considerable species specificity in terms of the interaction of HPr and IIA^{Mtl}. Thus, phosphoryl transfer between *E. coli* (Gram-negative) HPr and *S. carnosus* (Gram-positive) IIA^{Mtl} is ~10-fold lower than that involving *S. carnosus* HPr (70). Because the disposition of intermolecular hydrophobic interactions is preserved, the reduction in the rate of the heterologous phosphoryl transfer is presumably due to a reduction in the surface complementarity for the inter-species interactions. Thus, for example, *Phe-48* of HPr in the Gram-negative bacteria is substituted by *Met* in the Gram-positive bacteria (Fig. 4*C*) which will necessarily change the details of

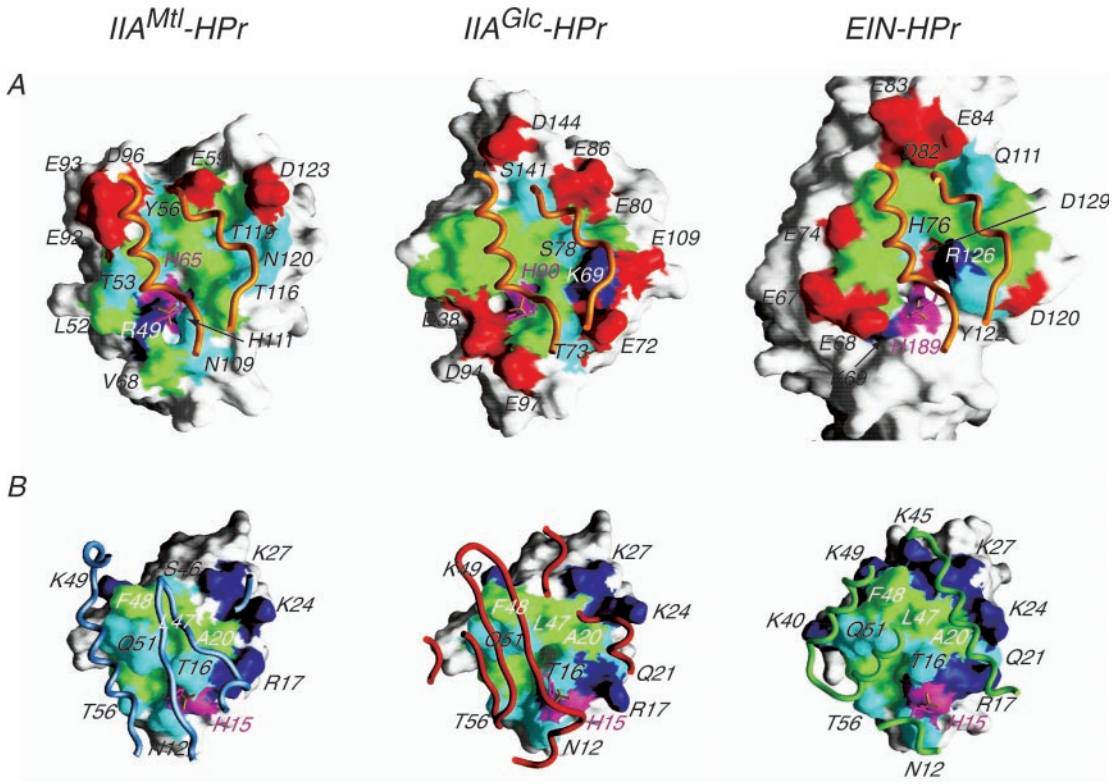

FIG. 6. **Surface representations illustrating the binding surfaces involved in the IIA^{Mtl}-HPr (*left panel*), IIA^{Glc}-HPr (*middle panel*), and EIN-HPr (*right panel*) complexes.** The binding surfaces on IIA^{Mtl}, IIA^{Glc}, and EIN are shown in *A*, and the binding surfaces on HPr are shown in *B*. The binding surfaces are color-coded with hydrophobic residues in *green*, polar residues in *light blue*, the active site histidines in *purple*, positively charged residues in *dark blue*, and negatively charged residues in *red*. The relevant portions of the backbone of HPr are shown in *gold* in *A*; the relevant portions of the backbone of IIA^{Mtl}, IIA^{Glc}, and EIN are shown in *blue*, *red*, and *green*, respectively, in *B*. The location of the phosphoryl group in the transition state is depicted in *yellow*. Residues of HPr are labeled in *italics*. The coordinates of the EIN-HPr and IIA^{Glc}-HPr complexes are taken from Garrett *et al.* (16) (code 3EZE) and Wang *et al.* (17) (code 1GGR), respectively.

the surface contour. As a consequence, there are compensatory changes in the hydrophobic residues of IIA^{Mtl} (at positions 57, 61, 119, 122, and 128; *cf.* Fig. 4*C*) that interact with *Met-48* that serve to maintain surface complementarity.

The Phosphoryl Transition State Intermediate—The phosphoryl group, originating on the Nδ1 atom of *His-15* of HPr (71, 72), is transferred to the Nϵ2 atom of His-65 of IIA^{Mtl} (59) with inversion of the configuration at phosphorus (73). This indicates a transition state involving a pentacoordinate phosphoryl group in a trigonal bipyramidal geometry, with the donor and acceptor nitrogen atoms of the active site histidines in apical positions and the oxygen atoms of the phosphoryl group lying in the equatorial plane (74).

We modeled the transition state using essentially the same approach as that described previously (17) in the case of the IIA^{Glc}-HPr complex; in particular, structures were recalculated introducing appropriate geometric restraints for the phosphoryl group in conjunction with all the experimental NMR restraints. Thus, the P-N distances were restrained to either 2 or 3 Å for associative (S_N2) and dissociative transition states, respectively; the phosphorus atom was restrained to lie in the plane of each imidazole ring. In addition, the backbone of the active site histidines and the adjacent residues on either side (*i.e.* residues 64–66 of IIA^{Mtl} and *14–16* of HPr) were allowed torsional degrees of freedom with their ϕ and ψ angles restrained by square-well potentials within $\pm$15 and $\pm$20°, respectively, of their values in the unphosphorylated complex. The results are displayed in Fig. 5*A*. The backbone r.m.s. difference between the mean coordinates of the structures calculated with and without the phosphoryl group is less than 0.1 Å, which is within the errors of the coordinates.

To accommodate the phosphoryl transition state, only small displacements (0.2 and 0.4 Å for the dissociative and associative transition states, respectively) in the backbone coordinates of the residues immediately adjacent to the active site histidines are required (Fig. 5*A*). This is mirrored by equally minor changes in backbone ϕ/ψ angles. The only noteworthy difference appears to be in the ϕ/ψ angles of *Thr-16* at the beginning of the first helix of HPr; these change from $-42/-67°$ in the unphosphorylated complex to the more helical values of $-65/-54°$ in the transition state complexes. The χ_1 and χ_2 rotamers of His-65 (g^+/g^-) of IIA^{Mtl} and *His-15* (g^+/g^+) of HPr remain unaltered. The χ_1 and χ_2 angles of His 65 changes by less than 5 and ~30°, respectively; the χ_1 and χ_2 angles of *His-15* change by 20–30 and ~1°, respectively. In addition, the side chain of Arg-49 is slightly displaced (~0.7–0.9 Å) by the presence of the phosphoryl group; this is achieved by very small changes (5–20°) in $\chi_1/\chi_2/\chi_3/\chi_4$ side chain torsion angles that remain in the $t/g^+/t/t$ rotamers.

A detailed view of the active site illustrating interactions that stabilize the transition state is shown in Fig. 5*B*. The phosphoryl group sits in a hydrophobic cleft comprising Leu-52, Ile-112, and Ile-115 of IIA^{Mtl}; there are no negatively charged carboxylate groups in close proximity. The phosphoryl group is within hydrogen bonding distance of the guanidino group of Arg-49 of IIA^{Mtl} and the hydroxyl group of *Thr-16* and the backbone amides of *Thr-16* and *Arg-17* of HPr. The *b* conformer of His-111 does not interact with the phosphoryl group, but its Nδ1 atom may be hydrogen-bonded to the carboxyamide of Asn-109; in the *a* conformer, the latter interaction is preserved but the Nϵ2 atom is now in close proximity to both the phosphoryl group and the side chain carboxyamide group of *Asn-12* of HPr. Although *Arg-17* of HPr does not participate in any electrostatic interactions with IIA^{Mtl}, it contributes to the pos-

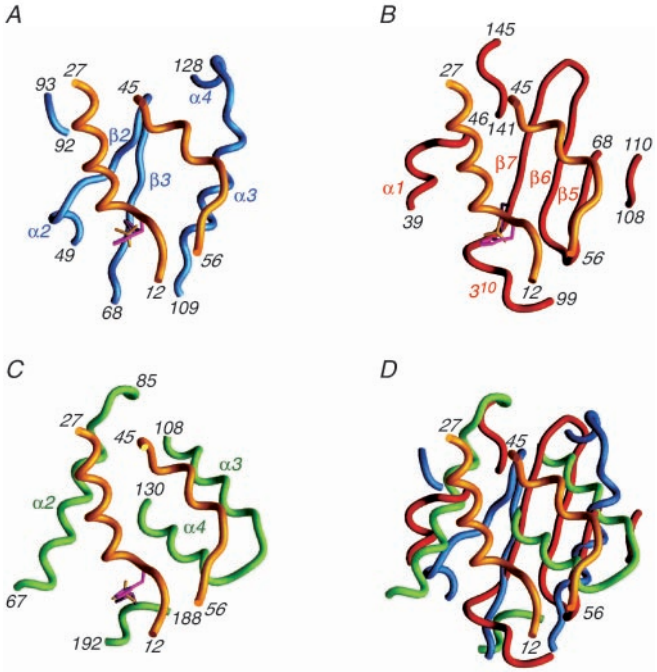

FIG. 7. **Comparison of the backbone structure of IIA^{Mtl}, IIA^{Glc}, and EIN comprising their respective interfaces with HPr.** *A*, IIA^{Mtl}-HPr; *B*, IIA^{Glc}-HPr; *C*, EIN-HPr complexes. *D*, best fit superposition (to HPr) of IIA^{Mtl}, IIA^{Glc}, and EIN in the three complexes. The backbones are shown as tubes with HPr in *gold*, IIA^{Mtl} in *blue*, IIA^{Glc} in *red*, and EIN in *green*. For reference, the side chains of the active site histidines are shown in *purple*, together with the phosphoryl in the putative phosphoryl transition states in *yellow*. The coordinates of the EIN-HPr and IIA^{Glc}-HPr complexes are taken from Garrett *et al.* (code 3EZE) (16) and Wang *et al.* (17) (1GGR), respectively.

itively charged environment in the vicinity of the phosphoryl group.

Comparison with the IIA^{Glc}-HPr and EIN-HPr Complexes—The interaction surfaces employed by HPr to recognize IIA^{Mtl} and IIA^{Glc} (17) and EIN (16) are very similar, overlap extensively, and consist of 17, 18, and 23 residues, respectively (Fig. 6*B*, *left*, *middle*, and *right panels*). Of the 17 HPr residues that participate in the IIA^{Mtl}-HPr complex, 15 are involved in the IIA^{Glc}-HPr complex and 16 in the EIN-HPr complex (Fig. 4*B*). In the case of the IIA^{Mtl}-HPr and IIA^{Glc}-HPr (17) complexes, the overall accessible surface areas buried at the interface are essentially the same (~1350–1450 Å^2) and distributed similarly between HPr (~45%) and the partner protein (~55%). The surface area buried at the interface of the EIN-HPr complex (16) is about 40% larger and approximately equally divided between HPr and EIN.

The backbone scaffolds comprising the interaction surfaces on IIA^{Mtl}, IIA^{Glc}, and EIN are topologically different both in terms of structure and connectivity: IIA^{Mtl} employs a mixture of helix and sheet (Fig. 7*A*); IIA^{Glc} predominantly makes use of sheet (Fig. 7*B*); and EIN uses only helices (Fig. 7*C*). Despite these differences, some elements of commonality can be observed (Fig. 7*D*). Thus, strands β3 of IIA^{Mtl} and β7 of IIA^{Glc}, which bear the active site histidine, are aligned; helix α3 of IIA^{Mtl} coincides with strands β5 and β6 of IIA^{Glc}; and helix α2 of IIA^{Mtl}, helix α1 of IIA^{Glc} and helix α2 of EIN partially overlap (Fig. 7*D*).

Surface representations of the interaction interfaces for the IIA^{Mtl}-HPr, IIA^{Glc}-HPr, and EIN-HPr complex are shown in Fig. 6 (*left*, *middle*, and *right panels*, respectively). The target surfaces that interact with HPr are broadly similar in all three cases comprising a central hydrophobic core located within a concave cleft surrounded by negatively charged residues (Fig. 6*A*). A number of electrostatic interactions are preserved in the three complexes. Thus, for example, *Gln51* of HPr is buried in all three complexes (Fig. 6*B*) and adapts its conformation to form potential hydrogen bonds with Thr-116 of IIA^{Mtl}, Ser-78 of IIA^{Glc}, and Arg-126 of EIN (Fig. 6*A*). Likewise, *Lys-49* of HPr forms potential salt bridges with Asp-123 of IIA^{Mtl}, Glu-80 and Glu-86 of IIA^{Glc}, and Glu-84 of EIN; *Lys-24* and *Lys-27* of HPr form potential salt bridges with Glu-92, Glu-93, and Asp-96 of IIA^{Mtl} and Asp-144 of IIA^{Glc}, and Glu-74 and Asp-82 of EIN. *Ser-46* of HPr interacts with a negatively charged residue in both the complexes with IIA^{Mtl} (Glu-59) and EIN (Asp-82), consistent with the finding that mutation of *Ser-46* to *Asp* significantly reduces activity for phosphoryl transfer to these two enzymes (75).

In addition to the similarities noted above, there are also a number of noteworthy differences between the three complexes. Although the negatively charged residues are almost uniformly distributed around the periphery of the interaction surfaces on IIA^{Glc} and EIN, they are clustered in essentially one region of IIA^{Mtl} (along the top rim of the interaction site in the view shown in Fig. 6*A*). From a structural perspective, this has consequences with regard to the role of the conserved *Arg-17* of HPr. *Arg-17* is critical for phosphoryl transfer between EIN and HPr and between HPr and IIA^{Glc} (76, 77), and its function is to neutralize a pair of negatively charged residues that are located in close spatial proximity to the active site histidines: Glu-67 and Glu-68 of EIN (16), and Asp-38 and Asp-94 of IIA^{Glc} (17) (Fig. 6, *A* and *B*). In the case of IIA^{Mtl}, these negatively charged residues are replaced by one positively charged residue, Arg-49, and two hydrophobic residues, Leu-52 and Val-68 (Fig. 6*A*, *left panel*). Thus, in the IIA^{Mtl}-HPr complex, the neutralizing role of the guanidino group of *Arg-17* is no longer required, and the aliphatic portion of the *Arg-17* side chain simply packs against the methyl groups of Leu-52 and Thr-53 (Fig. 4*A*). The guanidino group of Arg-49 of IIA^{Mtl}, on the other hand, forms a potential hydrogen bond with *Thr-16* in the unphosphorylated complex (Fig. 4*A*) and interacts with the phosphoryl group in the transition state (Fig. 5). This suggests that mutation of *Arg-17* to a neutral residue would have little impact on phosphoryl transfer between HPr and IIA^{Mtl}. This is borne out experimentally where mutation of *Arg-17* to His, Ser, Cys, or Gly has no effect on V_{max} and only increases K_m by a factor of ~2 (76). Mutation of *Arg-17* to a negatively charged residue (Glu), on the other hand, increases the value of K_m 100-fold, while leaving V_{max} unaltered (76); this is presumably due to either the introduction of a negative charge in close proximity to the phosphoryl group or possibly to a potential electrostatic contact with Arg-49, thereby hindering the interaction of Arg-49 with the phosphoryl group. Mutation of Arg-49 of IIA^{Mtl}, however, would be predicted to abrogate phosphoryl transfer between HPr and IIA^{Mtl}. This prediction is supported by the observation that Arg-49 appears to be absolutely conserved among IIA^{Mtl}s from different bacterial species (Fig. 4*C*).

The location of the active site histidines of IIA^{Mtl}, IIA^{Glc}, and EIN in the three complexes is also of interest. In the case of EIN (16), the active site His-189 is located at the very edge of the interaction surface, and adjacent residues in the sequence of EIN are not in contact with HPr (Fig. 6*A*, *right panel*). In contrast, in the case of both IIA^{Mtl} and IIA^{Glc}, the active site histidines, His-65 and His-90, respectively, are located just off-center of the interaction surface (Fig. 6*A*, *left* and *middle panels*, respectively). In all three complexes, the phosphoryl group in the transition state intermediate is located between the Nδ1 of *His-15* of HPr and the Nϵ2 atom of the active site histidine of the partner protein, and the χ_1/χ_2 angles of *His-15*

are in the same rotameric states (g^+/g^+). Consequently, the side chain conformation of the active site histidine of the partner protein must accommodate its different location relative to *His-15* of HPr in the three complexes. This is achieved by different combinations of rotameric states for χ_1 and χ_2: g^+/g^+ for His-65 of IIA^{Mtl}, t/g^- for His-90 of IIA^{Glc}, and t/g^+ for His-189 of EIN.

An example of conformational side chain plasticity is afforded by *Phe-48* of HPr. *Phe-48* participates in crucial intermolecular hydrophobic interactions in all three complexes (Fig. 6) and adapts its side chain rotamer conformation to optimize these; in the IIA^{Mtl} and IIA^{Glc} complex, the χ_1 angle of Phe-48 is in the *t* rotamer, whereas in the EIN complex it is in the g^- rotamer.

Concluding Remarks—The structure of the *E. coli* IIA^{Mtl}-HPr complex reveals that specificity is achieved through a large set of hydrophobic interactions, supplemented by a few electrostatic/hydrogen bonding interactions around the periphery of the interface. Comparison of the IIA^{Mtl}-HPr (this paper), IIA^{Glc}-HPr (17), and EIN-HPr (16) complexes show how HPr can use essentially the same interaction surface to recognize a plethora of structurally unrelated proteins. Three key factors are involved as follows: shape and residue complementarity of the interaction surfaces, even though the underlying backbone structural elements of the target surfaces are dissimilar; large interaction surfaces that can support redundancy of interactions and that minimize the effect of any single interaction (that is specificity is built up by a large series of interactions, each of which makes only a small contribution to the overall interaction energy); and side chain conformational plasticity to optimize intermolecular contacts and surface complementarity. These features are likely to be characteristic of many protein-protein interactions in signal transduction pathways that involve the rapid formation and dissociation of temporally transient, yet specific protein-protein complexes.

REFERENCES

1. Kundig, W., Ghosh, S., and Roseman, S. (1964) *Proc. Natl. Acad. Sci. U. S. A.* **52,** 1067–1074
2. Herzberg, O., and Klevit, R. (1994) *Curr. Opin. Struct. Biol.* **4,** 814–822
3. Postma, P. W., Lengeler, J. W., and Jacobson, G. R. (1996) in *Escherichia coli and Salmonella: Cellular and Molecular Biology* (Neidhardt, F. C., ed) pp. 1149–1174, American Society for Microbiology, Washington, D. C.
4. Tchieu, J. H., Norris, V., Edwards, J. S., and Saier, M. H. (2001) *J. Mol. Microbiol. Biotechnol.* **3,** 329–346
5. Robillard, G. T., and Broos, J. (1999) *Biochim. Biophys. Acta* **1422,** 73–104
6. Liao, D.-I., Kapadia, G., Reddy, P., Saier, M. H., Jr., Reizer, J., and Herzberg, O. (1991) *Biochemistry* **30,** 9583–9594
7. Worthylake, D., Meadow, N. D., Roseman, S., Liao, D.-I., Herzberg, O., and Remington, S. J. (1991) *Proc. Natl. Acad. Sci. U. S. A.* **88,** 10382–10386
8. Nunn, R. S., Markovic-Housley, Z., Genovesio-Taverne, G., Flükiger, K., Rizkallah, P. J., Jansonius, J. N., Schirmer, T., and Erni, B. (1996) *J. Mol. Biol.* **259,** 502–511
9. Sliz, P., Engelmann, R., Hengstenberg, W., and Pai, E. F. (1997) *Structure* **5,** 775–788
10. Van Montfort, R. L., Pijning, T., Kalk, K. H., Reizer, J., Saier, M. H., Thunnissen, M. M., Robillard, G. T., and Dijkstra, B. W. (1997) *Structure* **5,** 217–225
11. Van Montfort, R. L., Pijning, T., Kalk, K. H., Hangyi, I., Kouwijzer, M. L. C. E., Robillard, G. T., and Dijkstra, B. W. (1998) *Structure* **6,** 377–388
12. Eberstadt, M., Grdadolnik, S. G., Gemmecker, G., Kessler, H., Buhr, A., and Erni, B. (1996) *Biochemistry* **35,** 11286–11292
13. Ab, E., Schuurmann-Wolters, G., Reizer, J., Saier, M. H., Dijkstra, K., Scheek, R. M., and Robillard, G. T. (1997) *Protein Sci.* **6,** 304–314
14. Ab, E., Schuurman-Wolters, G. K., Nijlant, D., Dijkstra, K., Saier, M. H., Robillard, G. T., and Scheek, R. M. (2001) *J. Mol. Biol.* **308,** 993–1009
15. Schauder, S., Nunn, R. S., Lanz, R., Erni, B., and Schirmer, T. (1998) *J. Mol. Biol.* **276,** 591–602
16. Garrett, D. S., Seok, Y.-J., Peterkofsky, A., Gronenborn, A. M., and Clore, G. M. (1999) *Nat. Struct. Biol.* **6,** 166–173
17. Wang, G., Louis, J. M., Sondej, M., Seok, Y.-J., Peterkofsky, A., and Clore, G. M. (2000) *EMBO J.* **19,** 5635–5649
18. Reddy, P., Peterkofsky, A., and McKenney, J. (1989) *Nucleic Acids Res.* **17,** 10473–10488
19. Van Weeghel, R. P., Meyer, G. H., Keck, W., and Robillard, G. T. (1991) *Biochemistry* **30,** 1774–1779
20. Garrett, D. S., Seok, Y.-J., Peterkosfky, A., Clore, G. M., and Gronenborn, A. M. (1997) *Biochemistry* **36,** 4393–4398
21. Sondej, M., Weirglass, A. B., Peterkofksy, A., and Kaback, H. R. (2002) *Biochemistry* **41,** 5556–5565
22. LaVallie, E. R., DiBlasio, E. A., Kovacic, S., Grant, K. L., Schendel, P. F., and McCoy, J. M. (1993) *Bio/Technology* **11,** 187–193
23. Reddy, P., Fredd-Kuldell, N., Liberman, E., and Peterkofsky, A. (1991) *Protein Expression Purif.* **2,** 179–187
24. Delaglio, F., Grzesiek, S., Vuister, G. W., Zhu, G., Pfeifer, J., and Bax, A. (1995) *J. Biomol. NMR* **6,** 277–293
25. Garrett, D. S., Powers, R., Gronenborn, A. M., and Clore, G. M. (1991) *J. Magn. Reson.* **95,** 214–220
26. Clore, G. M., and Gronenborn, A. M. (1998) *Trends Biotechnol.* **16,** 22–34
27. Clore, G. M., and Gronenborn, A. M. (1991) *Science* **252,** 1390–1399
28. Bax, A., and Grzesiek, S. (1993) *Acc. Chem. Res.* **26,** 131–138
29. Bax, A., Vuister, G. W., Grzesiek, S., Delaglio, F., Wang, A. C., Tschudin, R., and Zhu, G. (1994) *Methods Enzymol.* **239,** 79–105
30. Hu, J.-S., and Bax, A. (1997) *J. Biomol. NMR* **9,** 323–328
31. Hu, J.-S., Grzesiek, S., and Bax, A. (1997) *J. Am. Chem. Soc.* **119,** 1803–1804
32. Rückert, M., and Otting, G. (2000) *J. Am. Chem. Soc.* **122**, 7793–7797
33. Ottiger, M., Delaglio, F., and Bax, A. (1998) *J. Magn. Reson.* **131,** 373–378
34. Chou, J. J., Delaglio, F., and Bax, A. (2000) *J. Biomol. NMR* **18,** 101–105
35. Losonczi, J. A., Andrec, M., Fischer, M. W., and Prestegard, J. H. (1999) *J. Magn. Reson.* **138,** 334–342
36. Zweckstetter, M., and Bax, A. (2000) *J. Am. Chem. Soc.* **122,** 3791–3792
37. Jia, Z., Quail, J. W., Waygood, E. B., and Delbaere, L. T. (1993) *J. Biol. Chem.* **268,** 22490–22501
38. Nilges, M., Gronenborn, A. M., Brünger, A. T., and Clore, G. M. (1988) *Protein Eng.* **2,** 27–38
39. Cornilescu, G., Delaglio, F., and Bax, A. (1999) *J. Biomol. NMR* **13,** 289–302
40. Schwieters, C. D., and Clore, G. M. (2001) *J. Magn. Reson.* **152,** 288–302
41. Clore, G. M., and Bewley, C. A. (2002) *J. Magn. Reson.* **154,** 329–335
42. Schwieters, C. D., Kuszewski, J., Tjandra, N., and Clore, G. M. (2002) *J. Magn. Reson.*, in press
43. Clore, G. M., Gronenborn, A. M., and Tjandra, N. (1998) *J. Magn. Reson.* **131,** 159–162
44. Clore, G. M., and Kuszewski, J. (2002) *J. Am. Chem. Soc.* **124,** 2866–2867
45. Kuszewski, J., Gronenborn, A. M., and Clore, G. M. (1999) *J. Am. Chem. Soc.* **121,** 2337–2338
46. Schwieters, C. D., and Clore, G. M. (2001) *J. Magn. Reson.* **149**, 239–244
47. Carson, M. (1991) *J. Appl. Crystallogr.* **24,** 958–961
48. Nicholls, A., Sharp, K. A., and Honig, B. (1991) *Proteins* **11,** 281–296
49. Schwieters, C. D., and Clore, G. M. (2002) *J. Biomol. NMR* **23,** 221–225
50. Altschul, S. F., Gish, W., Miller, W., Myers, E. W., and Lipman, D. J. (1990) *J. Mol. Biol.* **215,** 403–410
51. Jacobson, G. R., Lee, C. A., and Saier, M. H. (1979) *J. Biol. Chem.* **254,** 249–252
52. Lee, C. A., and Saier, M. H. (1983) *J. Biol. Chem.* **258,** 10761–10767
53. Stephan, M. M., Khandekar, S. S., and Jacobson, G. R. (1989) *Biochemistry* **28,** 7941–7946
54. White, D. W., and Jacobson, G. R. (1990) *J. Bacteriol.* **172,** 1509–1515
55. Van Weeghel, R. P., Meyer, G. H., Pas, H. H., Keck, W., and Robillard, G. T. (1991) *Biochemistry* **30,** 9478–9485
56. Lolkema, J. S., Kuiper, H., ten Hoeve-Duurkens, R. H., and Robillard, G. T. (1993) *Biochemistry* **32,** 1396–1400
57. Van Dijk, A. A., Scheek, R. M., Dijkstra, K., Wolters, G. K., and Robillard, G. T. (1992) *Biochemistry* **31,** 9063–9072
58. Kroon, G. J., Grotzinger, J., Dijkstra, K., Scheek, R. M., and Robillard, G. T. (1993) *Protein Sci.* **2,** 1331–1341
59. Pas, H. H., and Robillard, G. T. (1988) *Biochemistry* **27,** 5835–5839
60. Van Weeghel, R. P., van der Hoek, Y. Y., Pas, H. H., Elferink, M., Keck, W., and Robillard, G. T. (1991) *Biochemistry* **30,** 1768–1773
61. Tjandra, N., and Bax, A. (1997) *Science* **278,** 1111–1114
62. Tjandra, N., Omichinski, J. G., Gronenborn, A. M., Clore, G. M., and Bax, A. (1997) *Nat. Struct. Biol.* **4,** 732–738
63. Clore, G. M., Starich, M. R., and Gronenborn, A. M. (1998) *J. Am. Chem. Soc.* **120,** 10571–10572
64. Bax, A., Kontaxis, G., and Tjandra, N. (2001) *Methods Enzymol.* **339,** 127–174
65. Prestegard, J. H., and Kishore, A. L. (2001) *Curr. Opin. Chem. Biol.* **5,** 584–590
66. Clore, G. M. (2000) *Proc. Natl. Acad. Sci. U. S. A.* **97,** 9021–9025
67. Clore, G. M., and Garrett, D. S. (1999) *J. Am. Chem. Soc.* **121,** 9008–9012
68. Zweckstetter, M., and Bax, A. (2002) *J. Biomol. NMR* **23,** 127–137
69. Van Nuland, N. A. J., Kroon, G. J. A., Dijkstra, K., Wolters, G. K., Scheek, R. M., and Robillard, G. T. (1992) *FEBS Lett.* **315,** 11–15
70. Fischer, R., and Hengstenberg, W. (1992) *Eur. J. Biochem.* **204,** 963–969
71. Weigel, N., Powers, D. A., and Roseman, S. (1982) *J. Biol. Chem.* **257,** 14499–14509
72. Van Dijk, A. A., de Lange, L. C. M., Bachovchin, W. W., and Robillard, G. T. (1990) *Biochemistry* **29,** 8164–8171
73. Mueller, E. G., Khandekar, S. S., Knowles, J. R., and Jacobson, G. R. (1990) *Biochemistry* **29,** 6892–6896
74. Begley, G. S., Hansen, D. E., Jacobson, G. R., and Knowles, J. R. (1982) *Biochemistry* **21,** 5552–5556
75. Napper, S., Anderson, J. W., Georges, F., Quail, J. W., Delbaere, L. T. J., and Waygood, E. B. (1996) *Biochemistry* **35,** 11260–11267
76. Anderson, J. W., Pullen, K., Georges, F., Klevit, R. E., and Waygood, E. B. (1993) *J. Biol. Chem.* **268,** 12325–12333
77. Kruse, R., Hengstenberg, W., Beneicke, W., and Kalbitzer, H. R. (1993) *Protein Eng.* **6,** 417–423
78. Laskowski, R. A., MacArthur, M. W., Moss, D. S., and Thornton, J. M. (1993) *J. Appl. Crystallogr.* **26,** 283–291